IEEE Access
Multidisciplinary | Rapid Review | Open Access Journal

Received November 7, 2018, accepted December 14, 2018, date of publication December 20, 2018,
date of current version January 11, 2019.

Digital Object Identifier 10.1109/ACCESS.2018.2888912

dSPACE Controller-Based Enhanced Piezoelectric Energy Harvesting System Using PI-Lightning Search Algorithm

MAHIDUR R. SARKER, (Student Member, IEEE), RAMIZI MOHAMED, (Member, IEEE), MOHAMAD HANIF MD. SAAD, AND AZAH MOHAMED, (Senior Member, IEEE)

Center for Integrated Systems Engineering and Advanced Technologies, Faculty of Engineering and Built Environment, Universiti Kebangsaan Malaysia, Bangi 43600, Malaysia

Corresponding author: Mahidur R. Sarker (mahidur@ukm.edu.my)

This work was supported by the Ministry of Higher Education, Malaysia, under Grant GUP-2017-124 and Grant GGP-2017-011.

ABSTRACT This paper presents a new lightning search algorithm (LSA) to enhance the piezoelectric energy harvesting system converter (PEHSC) using the dSPACE DS1104 controller board as the proportional-integral voltage controller (PIVC). To extract the energy from the vibration is challenging and difficult due to the uncertain behavior of vibration. Since the piezoelectric vibration transducer generates low AC voltage output with fluctuations and harmonics, it is difficult to control this low-level signal of various magnitudes. Therefore, the behavior of the converter is governed by its controller. The traditional PIVC process for improved parameter values of proportional gain (Kp) and integral gain (Ki) is commonly implemented via trial and error, which does not lead to an acceptable response in several conditions. Hence, this paper offers a method for finding the optimal Kp and Ki values for PIVC that eliminates the time-consuming conventional trial-and-error process. This method is applied to PEHSC development by producing values of Kp and Ki performed in the PIVC depending on the estimated outcomes of the objective function defined via LSA. The mean absolute error (MAE) is used as the objective function for reducing the output error of the PEHSC. The LSA optimizes the Kp and Ki values that give the minimum MAE, and the effect on the PEHSC is in terms of the rising and settling times. The development process and efficiency of the PIVC are demonstrated and examined via simulations using the MATLAB tools. The LSA-based PIVC (LSA-PI) is compared with the particle swarm optimization (PSO)-based PIVC (PSO-PI) and the backtracking search algorithm (BSA)-based PIVC (BSA-PI). The performance of the LSA-PI-based PIVC is then validated through hardware implementation using the dSPACE DS1104 control board. The simulation results are compared with the hardware results of PEHSC to validate the overall efficiency of the system. Finally, the results are regulated at an output of 7 V DC from an input range of 150 mV∼250 mV AC at 30 Hz through a closed-loop using the LSA-PIVC.

INDEX TERMS Piezoelectric energy harvesting, dSPACE controller, PI controller, optimization.

I. INTRODUCTION

Currently, energy harvesting (EH) has become the key motivation of the energy sector, primarily because it is environmentally friendly, pure, and from a safe ambient source [1]–[3]. EH technologies are used to generate an electrical charge from various environmental waste and ambient sources, namely, water, waves, heat, solar and vibrations [4]–[7]. EH from numerous waste sources will be very popular due to the increasing demand for power. Among the possible natural energy sources, solar is stunning and a full-fledged technology. However, it has some drawbacks, such as a reduction in power delivery during foggy weather. This drawback becomes particularly important in remote regions where electronic devices are powered by solar energy and fully depend on solar power. On the other hand, to produce electrical charge using a thermoelectric EH source requires a large amount of heat. Therefore, the efficiency of vibrational sources is high due to its availability almost anywhere such as in home equipment, car engines, bicycles, roads, human movement, buildings, etc. EH using a

piezoelectric transducer from vibrational sources has been the main concern during the last few years. It has the potential of producing micro to milliwatts of power depending on the ambient conditions. The micro level EH becomes concentrated and is a focus of current researchers for powering the ultralow power devices in isolated regions [8].

The DC-DC converters such as the step-up, flyback, and step-down are the key to the piezoelectric EH system due to unstable low power sources [9]–[11]. Vibration-based piezoelectric EH generates a very low power from many sources, and it is not usable for low power electronic devices without increasing the voltage. Therefore, the main motivation for using the boost converter is to maximize the output voltage from the input voltage based on the desired output. The controlling efficiency of the boost in the open loop stage is very weak compared to that of the closed loop stage. However, the limitation of the open loop system boost converter is required to fix the input and output voltage based on the application. Moreover, the advantage of the closed loop system boost convert is the automatic delivery of the desired output voltage based on the application requirement, whatever the input voltage. In the single phase closed loop system, the DC-DC boost converter is required to control the MOSFET gate drive via a low or large frequency pulse width modulation (PWM). The benefit is a single-phase DC-DC boost converter in piezoelectric EH applications due to a low power loss probability, ease of implementation, and a low cost. Some previous studies have presented a switch mode DC-DC boost converter regulated by the duty cycle to accomplish the maximum outcome in the piezoelectric EH system [12]–[15]. The study in [14] developed a commercial step-up DC-DC converter ICs that increased the available voltage by 70 mV from the input voltage range of 200 mV to 500 mV, and the overall efficiency of the converter was 70%. The study in [12] proposed a DC-DC boost converter to enhance the output voltage for an EH system, and the model boosts up to 5.01 V DC with an input of 1.46 V and 2.19 V AC produced from piezoelectric energy harvesting devices. However, the converter efficiency and duty cycles were ignored in this study, and the results were primarily based on simulations without any hardware implementation. The work in [13] presented 0.13 μm piezoelectric energy harvesting devices using CMOS technologies to generate a 1.2 V stable DC voltage. However, the DC-DC converter shows weak voltage regulation and poor active response under an open loop condition. Therefore, a closed loop system boost converter is required to overcome the problem.

Many researchers have implemented a proportional integral derivative (PID) controller to improve the control structures in piezoelectric EH applications. PID control is used for consistent situation evaluation of a DC-DC step-up converter [16], [17]. This technique primarily depends on a consistent condition evaluation of the step-up converter using the condition area averaging approach and a low sign evaluation. This technique proposed the layout of an easy PID controller that can carry out to each step-up converter topology. PID control is used for the buck, boost and cuk DC-DC converters with the mode pick circuit [17]–[19]. The study in [17] proposed that the PID controller has various demerits including its need for mathematical modeling, excessive impressibility to parameter differences, a surprising alternate in the reference voltage, and the use of the trial-and-error approach. The complex segment is to search the suitable parameter values, namely, Kp and Ki. Normally, these parameter controls are used to guide tuning to achieve the suitable value, which requires a long time. Consequently, several techniques are used to determine PID parameters: the Ziegler-Nichols method [17], the Cohen-Coon method, the lambda tuning method, the visible loop tuning approach, and so forth. Unfortunately, these techniques are complicated by the issues of technique dissatisfaction, the use of trial-and-error, the need for a few calculation operations and a complex mathematical version [20]. Other optimization methods, namely, the genetic algorithm GA-PI optimization [21], PSO-PID optimization [22], and BSA-PI optimization, have been used to improve the behavior of the PI voltage controller (VC) and to find the parameters of the PI controller [23]. The LSA is an optimization method that has the benefit of steady robustness, a global convergence capability, and ease of implementation [24], [25]. To implement the optimization techniques on the controller, hardware control boards have been used including dSPACE, field programmable gate array (FPGA), microcontroller and eZdsp.

In this work, the LSA optimization method is proposed for tuning the optimal parameter values of the PI controller for PEHSC. A single dSPACE DS1104 controller board is used to control the PWM signal for low power PEHSC for different resistive loads. The dSPACE is used in some applications due to its quick counting, low power use, brief development period, and user-friendliness. The hardware outcomes represent the better behavior of the LSA-based PIVC. The remainder of this paper is organized as follows: Section 2 describes the development of the vibration-based PEHSC model. Section 3 presents converter control using the PI strategy. Section 4 presents the proposed PI voltage controller using optimization techniques for PEHSC. Section 5 presents a prototype implementation of the proposed controller for PEHSC. Section 6 provides the results and a discussion. Section 7 presents a comparison with existing methods, and finally, the conclusion is provided in Section 8.

II. DEVELOPMENT OF THE VIBRATION-BASED PEHSC MODEL

The proposed block diagram of vibration-based PEHSC consists of a piezoelectric vibration sensor, rectifier, low pass filter, boost converter, optimization technique, PI voltage controller and temporary storage device as shown in Fig. 1. The features of the proposed block diagram are described to develop PEHSC in this section. To improve the EH system, the optimization techniques used PIVC to search for the

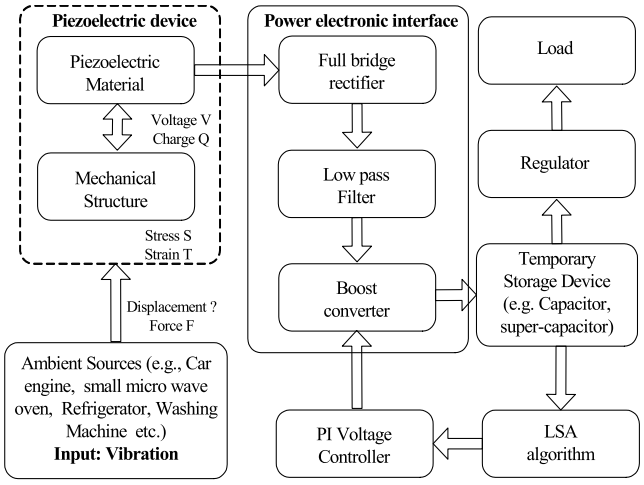

FIGURE 1. Proposed EH modules.

optimal values of Kp and Ki to enhance the performance of the proposed PEHSC.

A. PIEZOELECTRIC DEVICE

The effect of the piezoelectric transducer basically means an applied mechanical load is converted to electrical charge or voltage. On the other hand, the application of an electrical potential difference is converted to mechanical stress within the piezoelectric crystal.

B. MECHANICAL VIBRATION

The energy harvester model is equivalent to a damping mass-spring mechanical system with a transducer connected to an electrical interface circuit as presented in Fig. 2.

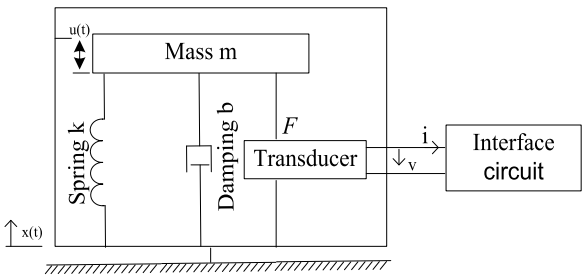

FIGURE 2. General model of a piezoelectric vibration energy harvester system.

The structure of the spring-mass-damping system for EH based on vibration consists of a mass m and a spring of stiffness k. Mechanical damping due to friction is represented by the damper b. An external vibration that is assumed to exert a sinusoidal force on the harvester body causes the body to move harmonically according to

$$x(t) = \hat{x}\sin(\omega t) \tag{1}$$

where $\hat{x}$ denotes the amplitude of the body in motion and ω denotes the natural vibration frequency. The analogous motion of the mass m with respect to the body movement is given by

$$u(t) = \hat{u}\sin(\omega t + \varphi) \tag{2}$$

where denotes $\hat{u}$ the amplitude of the mass motion and ϕ is the phase difference between $x(t)$ and $u(t)$. At the resonance frequency, there is a net displacement of $u(t)$ between the mass and structure, and the equation of motion of the mass system is defined by (3)

$$F = m\ddot{u} + b\dot{u} + ku \tag{3}$$

If the restoring force is considered an external force $F{=}ma$, equation (1) can be rewritten as

$$ma = m\ddot{u} + b\dot{u} + ku \tag{4}$$

$$ma = \ddot{u} + [\frac{b}{m}]\dot{u} + [\frac{k}{m}]u \tag{5}$$

where ma represents the external force that is exerted on the harvester, the excitation frequency is ω, and the natural frequency of the system is ω_n

$$\frac{b}{m} = 2\zeta\omega_n \quad \text{and} \quad \omega = \sqrt{\frac{k}{m}}, \quad \omega^2 = \frac{k}{m}$$

Therefore, equation (5) can be rewritten as

$$ma = \ddot{u} + 2\xi\omega_n\dot{u} + \omega^2 u \tag{6}$$

C. EQUIVALENT CIRCUIT OF THE ELECTRICAL MODEL

The electrical equivalent circuit of the vibration-based spring mass damping system described according to the electrical components is presented in Fig. 3. The mass m and inertia of the harvester are represented as an inductor L, the spring model as a capacitor C_o and C_s with the values *1/ko* and *1/ks*, respectively, that are inversely proportional, and the mechanical and electrical damping are denoted b with the resistor R. The electric equivalent circuit of a piezoelectric generator model can be described by applying Kirchhoff's current and voltage laws, referring to (7) and (8), respectively.

$$v(t) = L\frac{di}{dt} + \frac{1}{c_s}\int idt + \frac{1}{c_o}\int idt + Ri \tag{7}$$

$$i(t) = \frac{1}{L}\int vdt - \frac{1}{c_s}\int idt - \frac{1}{c_o}\int idt - Ri \tag{8}$$

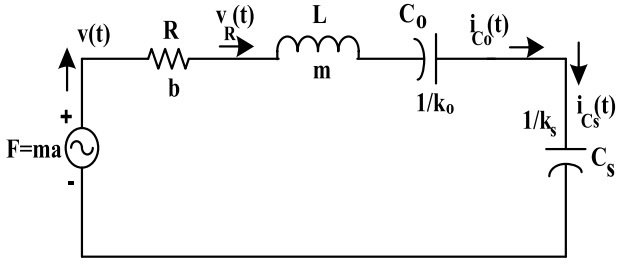

FIGURE 3. Equivalent circuit of the electrical model.

D. PIEZOELECTRIC DEVICE

The operation of a full-wave bridge rectifier requires four nodes connected with the bridge from *A*, *B*, *C* and *D* as shown in Fig. 4. It starts with node *D* attached with two diodes *D1* and *D3* at node *A*. Then, the remaining two diodes *D2* and *D4* are connected in series to terminate node *B*. The input AC supply is then connected to nodes *A* and *C*. The load resistances R_L are connected across nodes *D* and *B*. The input is provided from a piezoelectric bending generator (PBG) discharge sinusoidal wave. The positive half cycle of the circuit is determined between the period *t*, that is, *t=0* to *T/2*. Terminal *A* is positive with respect to terminal *C* so that the AC supply in the secondary side V_{ac} is positive. Therefore, *D2* and *D3* are forward biasing, whereas *D1* and *D4* are reverse biasing.

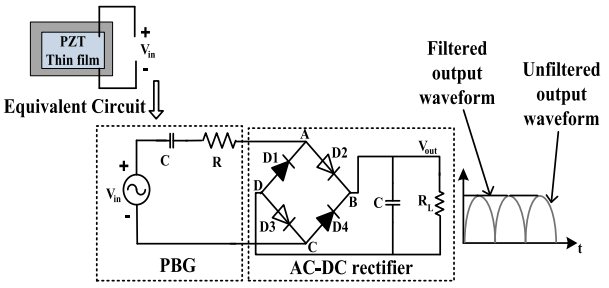

FIGURE 4. Operating modes of the proposed rectifier.

E. PIEZOELECTRIC DEVICE

Several studies have used the step-up DC-DC converter in a piezoelectric EH system [9], [26], [27]. Due to the low output voltage of the AC-DC rectifier generated from the PBG transducer, it is unsuitable for use without increasing the voltage. Therefore, a boost converter is required in a piezoelectric EH system and is used in the proposed system, as presented in Fig. 5. The principle of the boost converter is that the output voltage V_{out} is always greater than the input voltage V_{in} for a stable position process. This increases the voltage stage always upper. The structure of the converter consists of an inductor *L*, a MOSFET working as the gate drive to control the PWM, a diode *D1*, a filter capacitor *C*, and a load resistor R_L. The switching frequency is controlled via the switch *S* ON and OFF functions. When the switch is ON, then the duty ratio is the *D=ton/T* mode; moreover, another segment switch will be in the ON mode when the time interval is in the *ton* mode. On the other hand, the diode

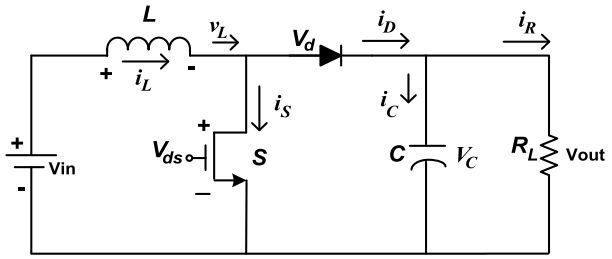

FIGURE 5. Typical circuit diagram for a DC-DC boost converter.

OFF mode depends on the time interval stage similar to the $0 < t \leq DT$ mode when the switch is in the ON position. The voltage throughout the inductor *L* is

$$V_{in} = v_L \tag{9}$$

$$V_{in} = L\frac{di_L}{dt} \tag{10}$$

Here, *L* is the inductance, and its value is calculated via equation (10). i_L is the current of the inductor.

$$\Delta I = \frac{V_{in}}{L}\Delta t \tag{11}$$

$$I_{\max} - I_{\min} = \frac{V_{in}}{L}DT \tag{12}$$

Here, the duty cycle (*D*) is the fraction of time in the overall period of the switching cycle (*T*) mode when the switch is in the ON position.

$$V_{in} = v_L + v_C \tag{13}$$

where the capacitor voltage V_{out} is combined with v_L. Once more, the inductor current is related to the inductor voltage to obtain

$$V_{in} = L\frac{di_L}{dt} + V_{out} \tag{14}$$

Equation (14) could be overcome via the transform current to obtain

$$\Delta I = \frac{V_{in} - V_{out}}{L}\Delta t \tag{15}$$

$$i_{\max} - i_{\min} = \frac{V_{in} - V_{out}}{L}(1-D)T \tag{16}$$

Combining (12) and (16) gives

$$-\frac{V_{in}}{V}DT = \frac{V_{in} - V_{out}}{L}(1-D)T \tag{17}$$

Simplifying (17) yields the capacitor voltage

$$V_{out} = \frac{V_{in}}{1-D} \tag{18}$$

$$D = 1 - \frac{V_{in}}{V_{out}} \tag{19}$$

The main function is to increase the output voltage of the boost converter while *D* is less than one and the output V_{out} is then greater than the input V_{in}. This is the basis of a step-up converter for increasing the voltage above the input voltage. The value of *D* plays a major role in boosting the voltage.

The mutual inductance of the boost converter, *L*, can be calculated using

$$L = \frac{D(1-D)^2}{2f_s} \tag{20}$$

where *L* is the maximum inductance of the converter, *D* is the maximum duty, and f_s is the switching frequency.

The total power loss of the converter is calculated as

$$P_{LS\_total} = P_{ML\_DS} + P_{DL\_D} + P_{L\_iL} \tag{21}$$

where is the resistance of the MOSFET.

The total diode conduction loss is represented by

$$P_{DL\_D} = P_{RF} + P_{VF} \tag{22}$$

where P_{RF} is the power loss in the diode forward resistance and is given as

$$P_{RF} = \frac{2R_F}{3}\sqrt{\frac{2(D-1)}{f_s LD}}P_{in} \tag{23}$$

where R_F is the diode forward resistance

$$P_{VF} = V_F I_p \tag{24}$$

where V_F is the diode threshold voltage and I_P is the input current of the PBG.

The inductor conduction loss is represented by

$$P_{L\_iL} = \frac{2r_L}{3}\sqrt{\frac{2D(D-1)}{f_s L}}P_{in} \tag{25}$$

where rL is the inductor resistor.

The working efficiency of the converter is calculated as

$$\eta = \frac{P_{in}}{P_{in} + P_{LS\_total}} \tag{26}$$

III. CONVERTER CONTROL USING THE PI STRATEGY

PI stands for proportional-integral. It describes a specific type of feedback controller in which the output is generally based on the error between the desired value (i.e., a user-defined set point) and a measured process variable. The main advantages of PI are its reliability, ease of implementation and lack of need for an equation model. This method of control uses the difference between the controlled variable set point and the controlled variable (error) multiplied by the controller gain and the integral action term to determine the required adjustment to be made to the manipulative variable [28]. The common pattern of the controller is tabulated in (27), and a block diagram is shown in Fig. 6.

$$Controller\ Output,\ O = K_p e + K_i \int_0^t edt \tag{27}$$

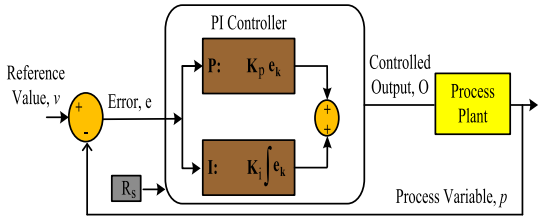

FIGURE 6. Model of the PI controller.

Here, Kp and Ki denote the proportional gain and integration gain, respectively, e represents the error, and t represents the time. In the PI voltage controller, gains such as Kp, Ki values are of major importance, and the efficiency of the controller is based on the gain performance. Therefore, selecting the appropriate values of gains is challenging. If the controller does not choose the proper values of Kp and Ki, then the output may display a large overshoot, fluctuate, and be unstable. However, there is a technique for selecting the proper values of the PI controller called the tuning method. Generally, to adjust the Kp, Ki value, use the tuning method and do it manually. This approach is time consuming and not successful in achieving the suitable value. Therefore, in this work, LSA optimization-based PIVC was considered to find the proper value due to its work automation and greater speed.

In view of the duration power conversion case in PEHSC, PIVC is a suitable technique to adopt in an EH converter control system. The PI controller is aimed at enhancing transient feedback and decreasing the unstable condition error of the boost controller when load disturbances occur. Fig. 7 shows the boost converter circuit control concept using PI as a control strategy. Here, L denotes the inductor and R denotes the resistor work as a load. Switch S is triggered by the pulse, which is generated via the PWM technique. The PWM technique receives Kp and Ki values from the PI controller and generates switching signals for the boost converter of the MOSFET for gate drives to deliver DC voltages to the PEHSC. An input voltage of the boost converter DC presents via V_{in} from the output of the rectifier circuit. The output of the boost converter denotes via V_{out} that it is higher than the input of V_{in}.

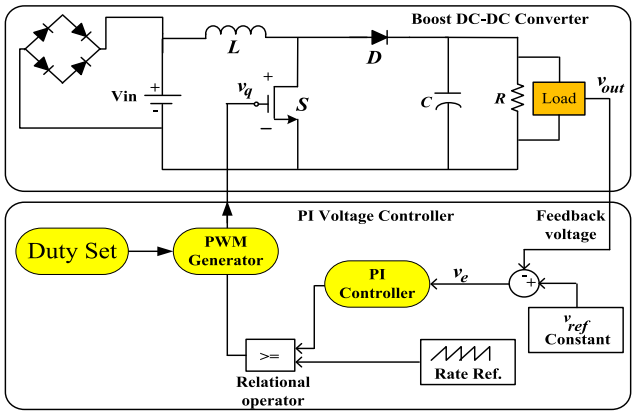

FIGURE 7. Converter voltage control using PI.

The control circuit consists of a PI controller, relational operator, PWM modulator, and a sawtooth voltage generator. A sum of the voltage error and its output gives the control signal v_q. The output signal V_{out} is compared with a reference voltage V_{ref}, and this gives an error voltage V_e, equal to

$$v_e = (v_{ref} - v_o) \tag{28}$$

IV. PROPOSED PI VOLTAGE CONTROLLER USING OPTIMIZATION TECHNIQUES FOR PEHSC

The standard PI controller design procedure is required for mathematical modeling and the trial-and-error technique. In addition, the difficult part of the PI controller is finding the best parameter values for Kp and Ki. Previously, manual tuning was needed to obtain the parameter values of

the controller, which was time consuming. Therefore, this study presents a methodology for optimizing the *Kp* and *Ki* parameter values using an optimization algorithm. The proposed LSA-PIVC circuit diagram simulation model for the PEHSC is designed using the PBG (as an input source), a bridge rectifier circuit, a low pass filter, a boost converter and temporary storage devices as presented in Fig. 8. The circuit works in a way that operation of PEHSC is input from PBG and its unstable low AC signal. A full-bridge rectifier circuit and filter is required to convert an AC signal to DC and to reduce the ripple. A boost converter is required to increase the rectifier voltage. If the switch of the MOSFET is cycled, the inductor will not discharge fully in between charging stages, and the load will have a larger voltage than the input source alone when the switch is opened. Then, the switch must be reopened sufficiently fast to prevent the capacitor from discharging. The drain (*D*) of the MOSFET wire connects with the inductor and diode. The source (*S*) of the MOSFET and diode connects with the capacitor. The input wire connects with the (*S*) of the MOSFET and the inductor. The gate (*G*) of the MOSFET connects with the DS1104 controller board ST2PWM as tabulated in Fig. 16, which generates the PWM signal from dSPACE. A comparison of the results from the MATLAB simulation and hardware implementation is provided in the results and discussion section. The PEHSC hardware implementation prototype board is shown in Fig. 18.

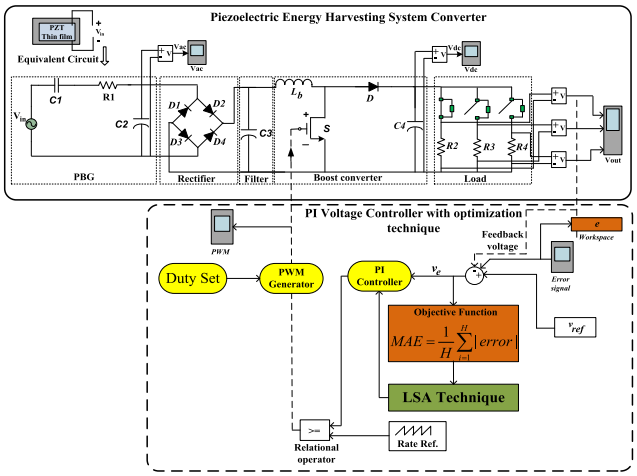

FIGURE 8. Circuit design of the proposed LSA-PI voltage controller for PEHSC.

A. LIGHTNING SEARCH ALGORITHM

Different optimization methods such as PSO, DSA, GA, BSA and the ant colony algorithm have been improved to raise the system efficiency by solving a real mathematical problem. However, these optimization methods have some limitations for solving complex mathematical optimization problems. The LSA is one of the latest optimization methods to be proposed to overcome these issues [24]. The LSA optimization method is founded on the structure of the step leader propagation of lightning as shown in Fig. 9. It regards the

FIGURE 9. Step leaders descending from a storm cloud.

engrossment of fast fragments recognized as projectiles in the structure of the binary tree creation of the step leader and in the synchronized creation of two leader instructions at split facts in place of a traditional spread management circulation. The LSA process is built on three steps: projectile and step leader propagation, projectile properties, and projectile modelling and movement. The projectile velocity is given by,

$$v_p = \left[1 - \left(\frac{1}{\sqrt{1-(v_0/l)^2}} - \frac{pF_i}{mc^2}\right)^{-2}\right]^{\frac{-1}{2}} \tag{29}$$

where v_p is current velocity of the projectile; v_o primary acceleration of the projectile; F_i is the steady lionization rate, l is the light speed; m is the mass of the projectile; and p is the length of the path travelled. The possibility consistency function $f(x^T)$ of the typical standardized allocation can be showed in equation below.

$$f(x^T) = \begin{cases} \dfrac{1}{(b-a)} & for\ a \le x^T \le b \\ 0 & for\ x < a\ or\ x^T > b \end{cases} \tag{30}$$

where x^T is an arbitrary value representing the initial tip energy, a is minor border of the solve area; b is higher border of the solve area. The current situation of the projectile is distributed via from the called augmented expanding handling with construct parameter μ. The probability densities function $f(X^S)$ of an exponential distribution is given by,

$$f(x^s) = \begin{cases} \dfrac{1}{\mu} e^{-\frac{x^s}{\mu}} & for\ x^s \ge 0 \\ 0 & for\ x^s \le 0 \end{cases} \tag{31}$$

where μ is construct parameter. In the LSA mechanism, μ is the distance between the lead projectile.

B. OPTIMAL PI VOLTAGE CONTROLLERS

The optimization approach includes three vital capabilities, namely, input records, an objective feature and optimization barriers. Each component runs for improvement and association to obtain optimal PI parameter values. The optimization approach gains a suitable outcome by reducing the objective function via the input data and the gathering of the barriers in each creation of the iterative method.

1) INPUT INFORMATION

In the beginning of PI voltage controller development, the values of Kp and Ki must be determined to offer the outcome from the optimization method. Based on the number of parameter values of the PI voltage controller, the input vector Z is given as:

$$Z_{i,j} = \left[Y_{i,j}^{1} Y_{i,j}^{2} ... Y_{i,j}^{n} \right] \tag{32}$$

Here, $Z_{i,j}$ denotes the j_{th} outcome in the population during the i_{th} iteration, Y is a component of $Z_{i,j}$, and n is the number of parameters. In this work, two problem dimensions and a population of 30 have been considered to obtain the suitable parameter values for the PIVC.

2) OBJECTIVE FUNCTION

An objective function is crucial for the optimization approach to gain reducing error. Therefore, the goal of the objective function is to obtain a suitable value for the PIVC output to enhance the device balance. The MAE is used as an objective function to find suitable parameter values for the controller for great outcomes. The objective function MAE is calculated using equation (33).

$$MAE = \frac{1}{H} \sum_{i=1}^{H} |error| \tag{33}$$

where H represents the amount of trial and error in the PIVC for the step-up converter. In the optimization method, equation (33) needs to be reduced.

3) OPTIMIZATION CONSTRAINTS

The optimization method should be executed and used to determine the optimal values of the K_p and K_i parameters. The borders of these parameters should not overlap. On the other hand, the variable $X_{i,j}^{k}$ should be between $X_{i,j}^{k-1}$ and $X_{i,j}^{k+1}$. If $X_{i,j}^{k}$ is greater than $X_{i,j}^{k+1}$ or less than $X_{i,j}^{k-1}$, it should be reproduced within its borders. Hence, the following constraint must be satisfied to confirm that K_p and K_i are within the appropriate borders.

$$X_{i,j}^{k-1} < X_{i,j}^{k} < X_{i,j}^{k+1} \tag{34}$$

4) OPERATION STEPS OF LSA TO GAIN THE OPTIMAL PEHSC DEVELOPMENT

The performance is initiated by rearranging the LSA parameters, such as the number of iterations (I), population size (S), problem dimension (P), projectile energy E_p, step leader energy Esl and channel time. The elementary populations for Kp and Ki are produced and presented corresponding to equation (32). The other part includes the assessment of the objective function via equation (33). After the elementary population is estimated, the govern and place are improved with equations (35) and (36), accordingly: before improving each value of $Z_{i,j}$ in the population, the generator re-assesses the objective function, and the operation continues to the next iteration

$$p_{i\_currrent}^{S} = p_{i}^{S} \pm \exp\ rand\ (\mu_i) \tag{35}$$

$$p_{i\_current}^{S} = p_{i}^{S} \pm \exp\ rand\ (\mu_i) \tag{36}$$

where $p_{i\_current}^{S}$ is the current space projectile, P_{i}^{S} is the previous space projectile, and $p_{current}^{L}$ is the current lead projectile. Before improving each value of $Z_{i,j}$ in the population, the generator re-assesses the objective function, and the procedure continues to the next iteration. This improving and objective function reassessment procedure is repeated until the highest iteration count is achieved, as illustrated in Fig. 10.

The optimal PIVC utilizing LSA is compared with optimal PIVC utilizing PSO which is an optimization method based on population of swarm motion. The PSO algorithm also utilized the same parameters as that utilized for LSA for comparison. The parameters utilized in PSO are the number of iterations (I) = 500, population size (S) = 30, problem dimension (P) = 2. The procedure in PSO starts by generating and encoding the initial population according to equation (34). Thereafter, the initial population is evaluated by using equation (33). The BSA algorithm also utilized the same parameters as that utilized for LSA for fair comparison. So, the parameters utilized in BSA are that the number of iterations (I) = 500, population size (S) = 30, problem dimension (P) = 2.

V. PROTOTYPE IMPLEMENTATION OF THE PROPOSED CONTROLLER FOR PEHSC

Prototype architecture is the demonstration of a digital system, technique and manipulation for enforcing the layout for the type of prototype system. Usually, it is a segment of an incorporated device including the circuit statistics and software program for developing a tool prototype. To test and verify the performance of the circuit hardware, implementation plays a major role. For that reason, it is important to verify the system via hardware implementation before use in real applications. The implementation of the optimum PI voltage controller for PEHSC using the DS1104 control board is described in this section. The PEHSC model and control algorithm are developed and simulated in the MATLAB/Simulink environment and then linked to the converter using the DS1104 controller board. The experimental setup for implementing the optimum PIVC for PEHSC is presented.

This section presents the hardware development of the signal-phase PEHS converter and the control algorithm, as well as the necessary hardware for integration with the dSPACE DS1104 controller system. In addition, it describes the experimental setup of the integrated PEHSC prototype.

A. PIEZO BENDING GENERATOR

The PBG acts as a bending mechanical shape that generates a quantity of energy from pressure. PEHSC was examined via a single PBG. The block diagram of the PBG is given in Fig. 11. The function of the PBG requires pressing using vibrational

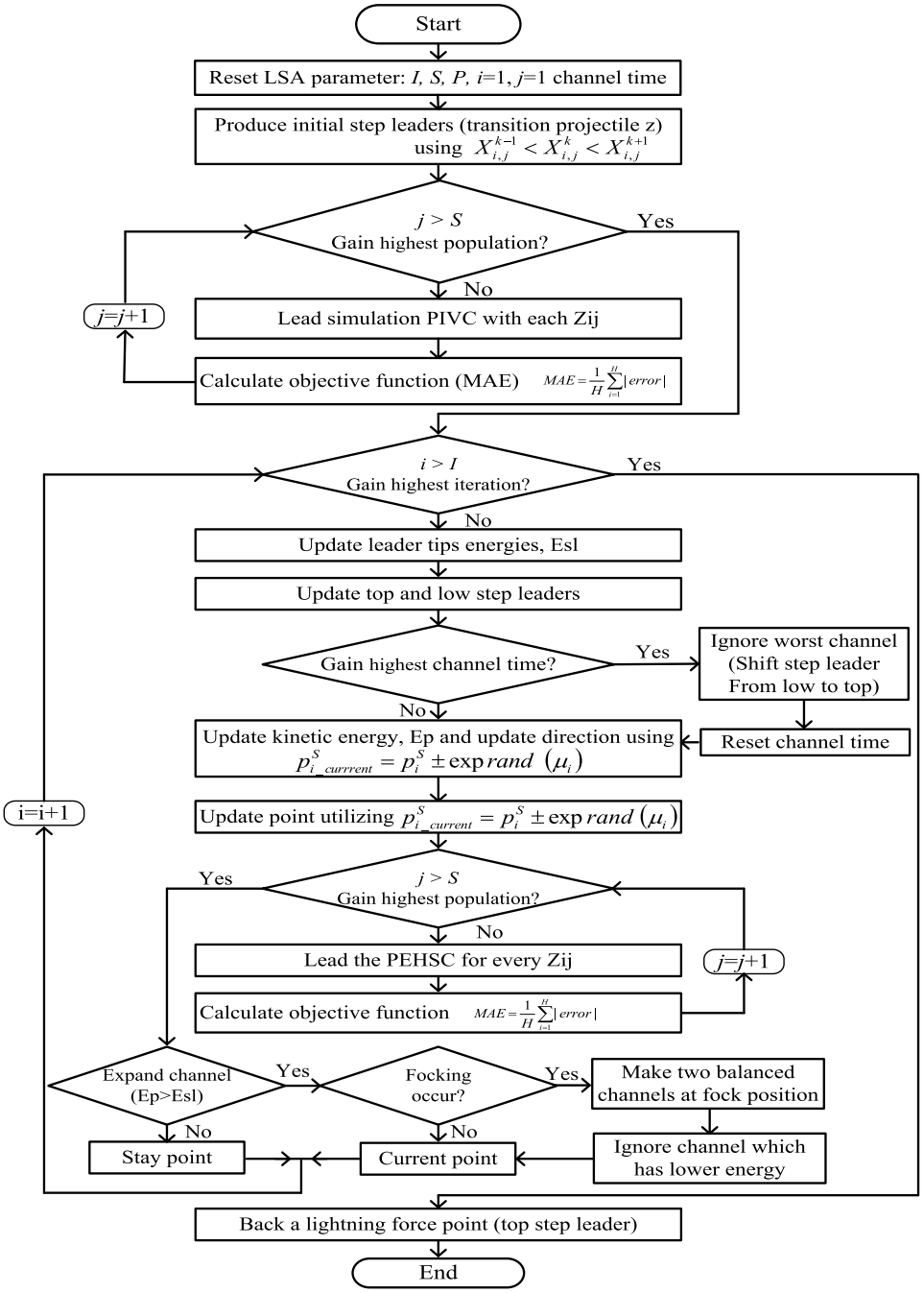

FIGURE 10. Proposed LSA-based optimum PI voltage controller design procedure.

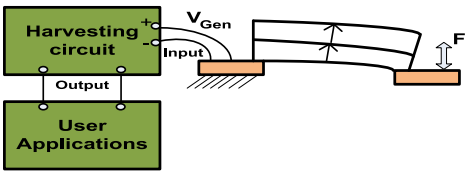

FIGURE 11. Block diagram of the PBG.

pressure. While one part of the PBG is fixed, the alternative surface is free to move. While the PBG vibrates, its electrodes collect an amount of energy that overlooks to prevent the forced stress. This energy is harvested, saved, and added to the EH circuit. The PBG communicates with an EH interface circuit that extracts charge and adds it to a storage element, which includes a rechargeable battery or a supercapacitor.

B. EXPERIMENTAL SETUP OF THE PBG

The PBG is a vibration transducer with a two layer binding generator that produces a low power charge via vibration stress. Operating the PBG requires a vibration shaker and amplifier module. One side of the PBG is attached to a

vibration shaker that operates through the amplifier module. The block diagram and experimental test bench layout are presented in Fig. 12. To perform the PBG analysis, the natural frequency was varied between 10 Hz and 60 Hz via the amplifier unit. An investigation of the resonance frequency of the PBG is presented in the results and discussion section.

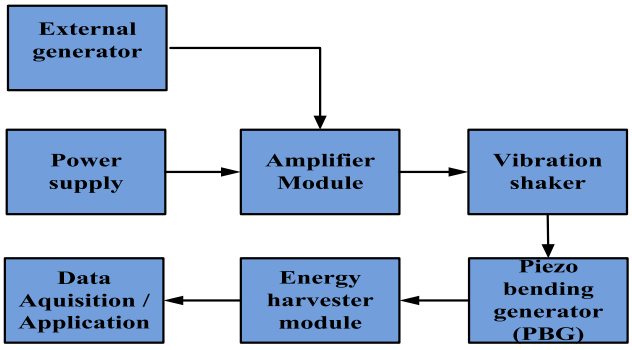

FIGURE 12. Block diagram of the experimental test bench layout.

C. HARDWARE IMPLEMENTATION VIA DS1104 CONTROLLER BOARD BASED ON LSA

The MATLAB Simulink tools depend on the dSPACE controller board in real-time implementation, which is a popular platform in academic research. dSPACE is a famous controller board, offering many advantages in terms of monitoring, controlling, and automating experiments and making the improvement of controllers more efficient. The DS1104 controller board with the best response in terms of a high memory space and faster implementation process was considered in this study. The properties of the DS1104 controller board are explained in Fig. 13. This figure shows the general connection of the controller board with the personal computer and the converter (hardware). A photo of the DS1104 controller board is shown in Fig. 14, and the implementation flow of the dSPACE-based converter system is presented in Fig. 15.

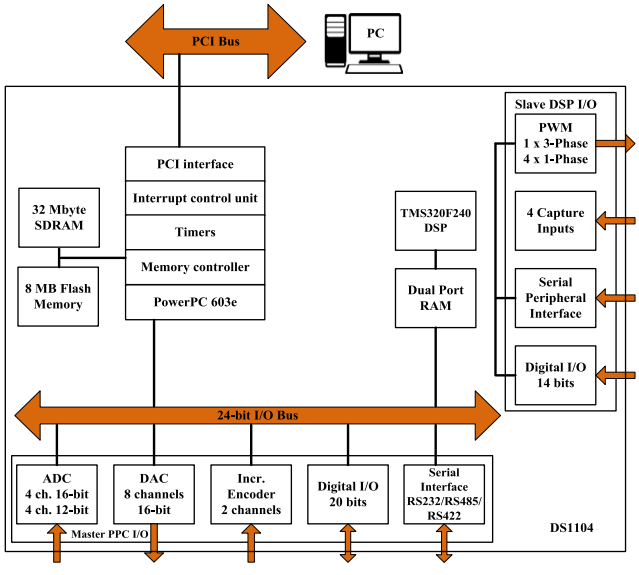

FIGURE 13. Block diagram of the DS1104 controller board.

FIGURE 14. Photo of the DS1104 controller board.

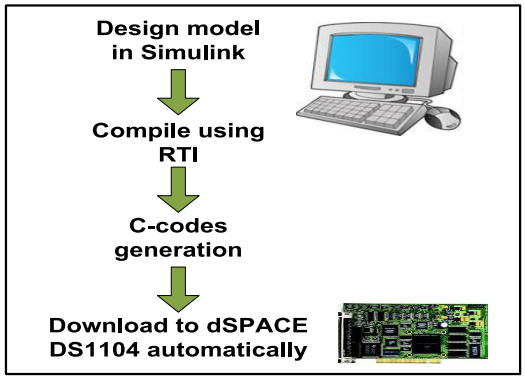

FIGURE 15. Flow of the implementation of the dSPACE-based converter system.

Real-time interface (RTI) is the real-time adoption software for the dSPACE scheme that enhances the real-time C-code automation, faultlessly effects the dSPACE system and input/output hardware structure, and automatically creates, accumulates, connects, and performs the real-time C-code from the Simulink structure [29]. Moreover, RTI produces a variable file corresponding to signals and parameters, and ControlDesk will contact this file and update the parameters [29]. With RTI, one may simply run the function models on the DS1104 controller board. It configures each I/O graphically by pulling RTI blocks and decreases the implementation time to a minimum.

The DS1104 enhances personal computers (PCs) with a strong improvement scheme for faster control implementation. RTI produces Simulink blocks for the graphical structure of an analog-to-digital converter (ADC), a digital-to-analog converter (DAC), I/O lines, and PWM. Generally, the board may be installed in each PC with a free 5-V peripheral component interconnect (PCI) slot.

There is a requirement for the signal conditioning circuits to be processed via the dSPACE controller board before feeding the signal. This requirement ensures that the voltage

and current signals are specified in such a way that the levels match the ADC input range of the controller. Depending on the level condition of the input, the signal undergoes the process of reduction, amplification or current-to-voltage conversion. The signal conditioning consists of AC voltage and current conditioning circuits, and DC voltage conditioning, as depicted in Fig. 16.

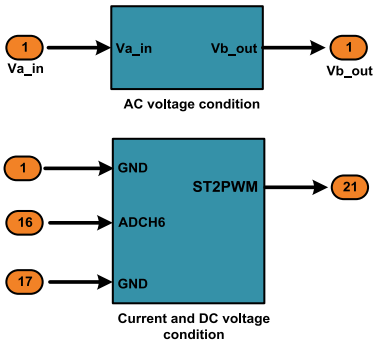

FIGURE 16. Signal conditioning.

The computer must be prepared with the dSPACE-associated software and hardware, namely, the ControlDesk (dSPACE 2008) software and the DS1104 controller board. Some of the parameters must be measured or tested properly to be set as inputs to the controller. For this purpose, the measurement and dissipation circuits are required. The proposed control algorithm, which is the LSA optimization based on PIVC, is implemented in the dSPACE DS1104 controller board as described in Fig. 17.

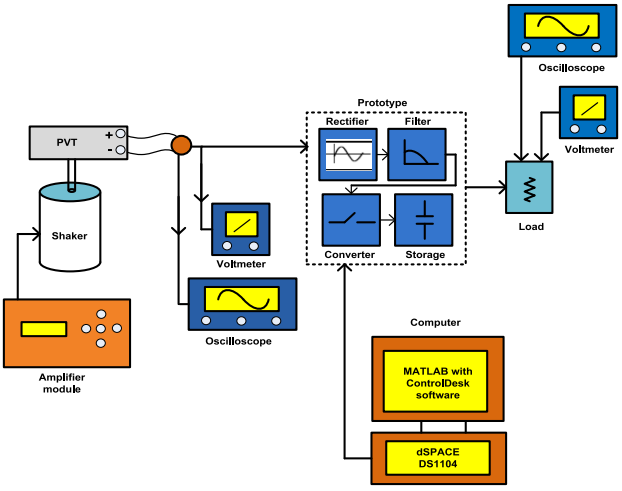

FIGURE 17. Block diagram of the experimental setup.

The implementation of the MATLAB/Simulink converter control technique simulated in real time is proficient with the use of the dSPACE DS1104 RTI. In doing so, the required dSPACE input-output library blocks are involved in the control technique. Fig. 18 shows the real-time implementation of the dSPACE converter system techniques.

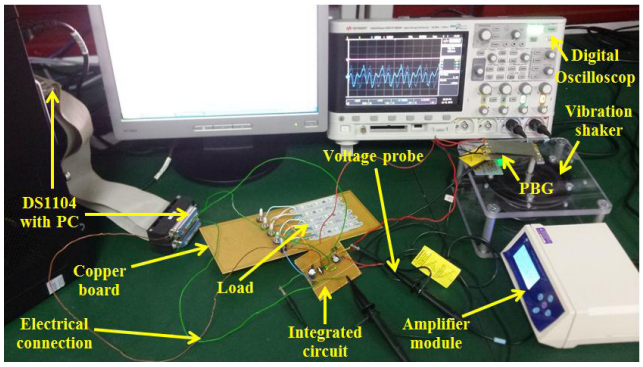

FIGURE 18. dSPACE-based PEHS prototype implementation in-lab experimental setup.

VI. RESULTS AND DISCUSSION

This section describes the optimal outcomes of the LSA-PI, BSA-PI and PSO-PIVC methods of PEHSC.

A. DATA EXTRACTING FROM THE PBG

This experiment was performed to achieve the behavior of the PBG using EH components such as a vibration shaker and amplifier unit. Using which amplitude and frequency the PBG will shake, it can easily be controlled manually via an amplifier module to produce the vibration signal at various frequency ranges. The experimental output of the PBG is tabulated in Table 1. Fig 19 shows the measurement of the AC Vpp voltage of the PBG at different frequencies. The frequency spectrum graph is tabulated in Fig. 20. Fig. 20 presents the voltage amplitude of the PBG behaviors according to the frequency without the load. The response of the PBG was analyzed with the maximum peak above 70.7% and the selected resonance frequency (i.e., 30 Hz, 40 Hz, 60 Hz) that generated the maximum V_{pp} voltage. The resonance frequency of 30 Hz was selected from the PBG that generated the maximum amplitude for the development of the simulation and experimental models for PEHSC.

TABLE 1. Analytical data from the PBG.

Frequency (Hz)	Vpp
10	1.63
18	2.35
24	4.63
30	7.2
32	1.96
38	2.67
40	5.16
43	3.1
48	2.85
50	2.97
52	4.20
54	5
58	3.09
60	6.4

B. LSA PERFORMANCE

The proposed LSA is applied to a group of three objective functions. This section describes the optimal outcomes of the LSA-PI, BSA-PI and PSO-PIVC methods of PEHSC.

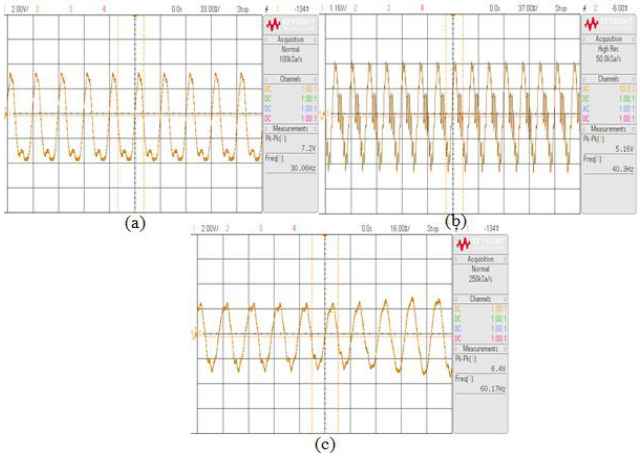

FIGURE 19. Measurement of the AC Vpp voltage for the PBG frequency of (a) 30 Hz, (b) 40 Hz, and (c) 60 Hz.

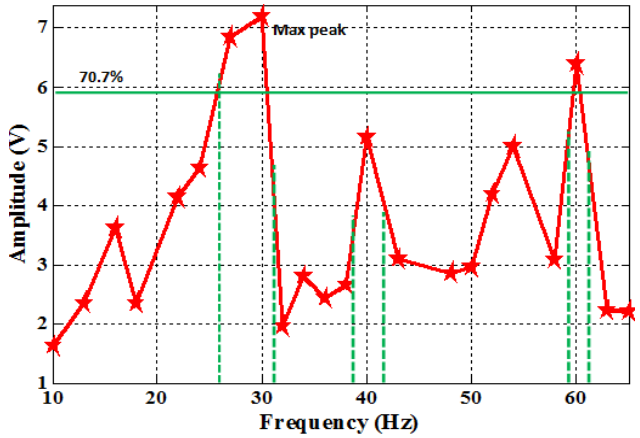

FIGURE 20. Frequency spectrum of the PBG.

1) EVALUATION OF LSA, BSA AND PSO BASED ON THE OPTIMUM PIVC

The performance of the optimum PIVC using LSA (LSA-PI) is compared with that of the BSA (BSA-PI) and PSO (PSO-PI) optimization techniques. The PIVC parameters were successfully adjusted via the LSA optimization method to obtain the optimal (Kp, Ki) parameter values for the PI. The LSA optimization algorithm achieved the smallest error for the MAE objective function. To assure that the assessments are clean, the population size and maximum iteration for each optimization technique that was tested with all methods are tabulated in Table 2. Finally, to validate the objective function such as MAE, the root mean square error (RMSE) and standard deviation (SD) of the error are used to evaluate LSA-PI, BSA-PI, and PSO-PI. The MAE is given by (37), and the other two indices are given in [30] by (38) and (39).

$$MAE = \frac{1}{H}\sum_{i=1}^{H}|e_r| \tag{37}$$

$$RMSE = \sqrt{\frac{1}{l}\sum_{r=1}^{H}e_r^2} \tag{38}$$

$$SD = \sqrt{\frac{1}{l}\sum_{r=1}^{H}(e_r-\eta)^2} \tag{39}$$

where H is the sample error in the PIVC for PEHSC, l is the number of samples, and η is the average error value.

TABLE 2. Parameter settings used in LSA, BSA, and PSO.

Parameter	LSA	BSA	PSO
Population Size	30	30	30
Max. Iteration	500	500	500
c1 and c2	-	-	1.5
F	-	3	-
Channel time	10	-	-

2) SIMULATION AND HARDWARE OUTCOMES OF THE PROPOSED SIGNAL-PHASE PEHSC USING LSA-PIVC

This section describes the output of the enhancement effects of the LSA optimization-based PIVC for the PEHSC. For proof, the outcomes of the PEHSC simulation were compared with the outcomes of the experiment. The PI voltage controller parameters were correctly tested with the aid of the LSA optimization method to achieve the optimal (K_p, K_i) parameter values for the PI. This system was also conducted via the BSA and PSO optimization methods to obtain the most effective PI parameter. This contrast is used to measure and outline the robustness of the LSA optimization method. Fig. 21 shows the optimization behavior of the LSA-PI, BSA-PI, and PSO-PI methods using the objective function of MAE for 500 iterations. The LSA-PI optimization approach obtains the minimum objective function MAE values. Table 3 presents the output error from various methods for the MAE objective function. It is clearly shown in Table 3 that the LSA method generates the smallest error.

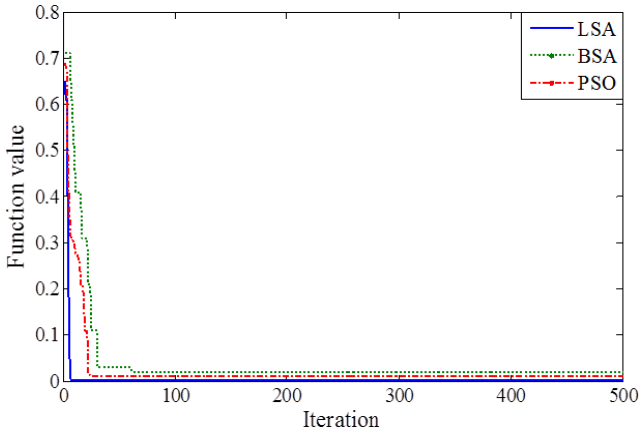

FIGURE 21. Convergence curves for LSA, BSA, and PSO for the objective function MAE.

TABLE 3. Values of the output error via several methods.

MAE	LSA	BSA	PSO
	0.000000000099454	0.01035454	0.019999999

C. MOSFET PWM SWITCHING SIGNALS

The generation of control signals for switching devices is the key element in converter control systems. A PWM signal is an example of a control signal that switches the MOSFET ON and OFF, which in turn shapes-up the converter output waveform. Therefore, it is important to understand and recognize the shape and pattern of these signals. In this section, the PWM control signals are recorded for the system performance comparison and assessment. To turn ON the MOSFET and produce the DC output voltage at its output terminal, a PWM signal is supplied to the gate terminal of the MOSFET.

The comparison of the generated PWM switching signal of the simulation and experiment is illustrated in Fig. 22 (a) and (b). From these figures, it is clear that a switching frequency of 10 kHz and a period for one cycle of PWM of 10 μs are calculated to implement the prototype of the PEHSC. By observing the signal pattern, it can be concluded that the duty cycle of the PWM cycle is increasing. This can be observed by the width of the pulses. Notably, in the simulation, the control signal is in the digital form of a '0' and '1' level. The first digit causes a switching device to turn ON, whereas the second one tends to switch it OFF.

D. COMPARISON OF SIMULATION AND HARDWARE OUTCOMES OF A PEHSC

This work analyzed and compared the simulation and hardware outcomes of a PEHSC input and output voltage using the proposed method. These sections analyze, justify and compare the effectiveness of the developed converter control system for PEHSC based on the rising and settling times, stability, boost maximum voltage and response speed under various input conditions.

1) SIMULATION AND EXPERIMENTAL RESULTS BASED ON THE SETTLING TIME AND RISING TIME WITH AN INPUT OF 150 MV

To approve the optimization outcomes, the performance of LSA-PI is verified with BSA-PI and PSO-PI. The feedback of the PEHSC simulation outcomes using the PSO-PI, BSA-PI and LSA-PI controllers is presented in Fig. 23. From Fig. 23, it is observed that LSA-PI can obtain a suitable optimal result in terms of the rising time, which is less than that of the BSA-PI and PSO-PI controllers, and the settling time is longer for BSA-PI and PSO-PI but shorter for LSA-PI. The outcomes of the hardware agreed clearly with the simulated results as presented in Fig. 24. Table 4 compares the optimized output using these methods. The LSA-PI effectively achieved the goal with suitable outcomes verified via the BSA-PI and PSO-PI controllers based on the settling and rising times.

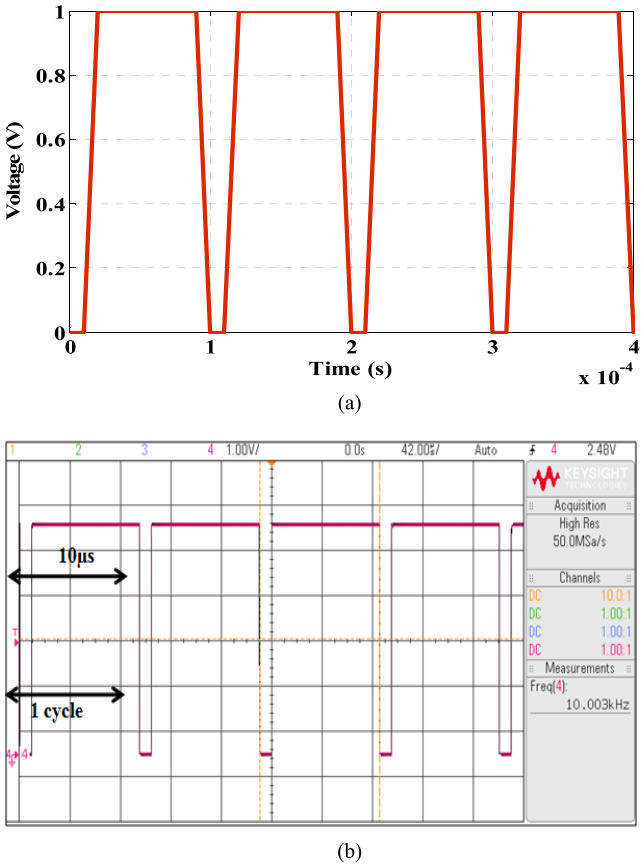

FIGURE 22. (a) PWM simulation switching signal of the MOSFET gate. (b) PWM experimental switching signal of the MOSFET gate.

TABLE 4. Comparison results obtained using the LSA-PI, BSA-PI and PSO-PI controllers with an input of 150 mV.

Algorithms	Rise Time	Settling Time	Peak over shoot	Steady state Error
LSA-PI	0.051 s	0.099 s	0%	0.1
BSA-PI	0.132 s	0.252 s	0%	0.1
PSO-PI	0.151 s	0.351 s	0%	0.1

2) SIMULATION AND HARDWARE OUTCOMES OF PEHSC WITH AN INPUT OF 150 MV

The simulation results using the LSA-PI, BSA-PI and PSO-PI approaches are presented in Fig. 25 (a), (b) and (c), respectively. Fig. 25 (a) shows that the PBG produced an AC sinusoidal Vrms of 150 mV and a stable boost up 7 V DC without any ripple via the proposed LSA-PI method of the PEHSC. Primarily, the curve bends, but after 0.099 s, it becomes stable. Conversely, Fig. 25 (b) and (c), shows that the outcomes of the BSA-PI and PSO-PI methods are almost comparable in terms of the input and output voltage behaviors, but the curve becomes stable after 0.252 s and 0.351 s for BSA-PI and PSO-PI, respectively. The peak overshoot value is almost comparable for the three methods. The experimental outcome agrees with the simulated outcome shown in Fig. 26 (a), (b) and (c). A comparison between the simulation and the hardware implementation results of PEHSC is provided in Table 5.

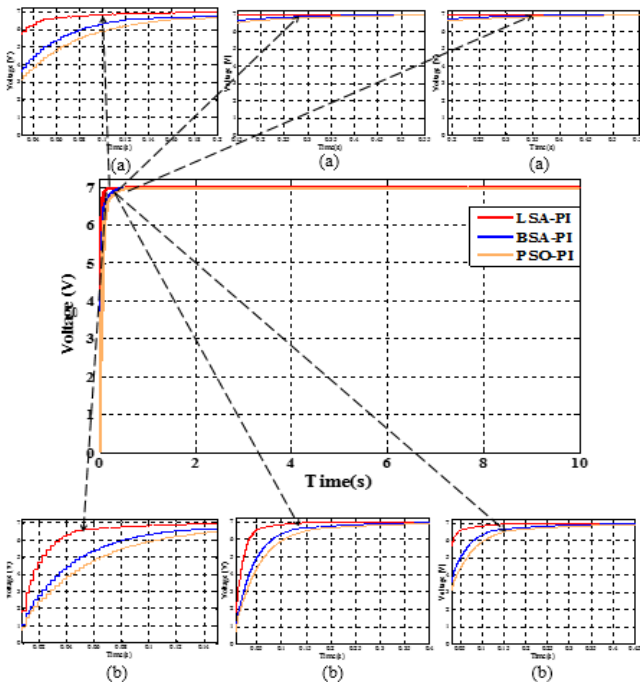

FIGURE 23. Simulation results of the LSA-PI, BSA-PI and PSO-PI controllers based on the rise time (a) and settling time (b) with an input of 150 mV.

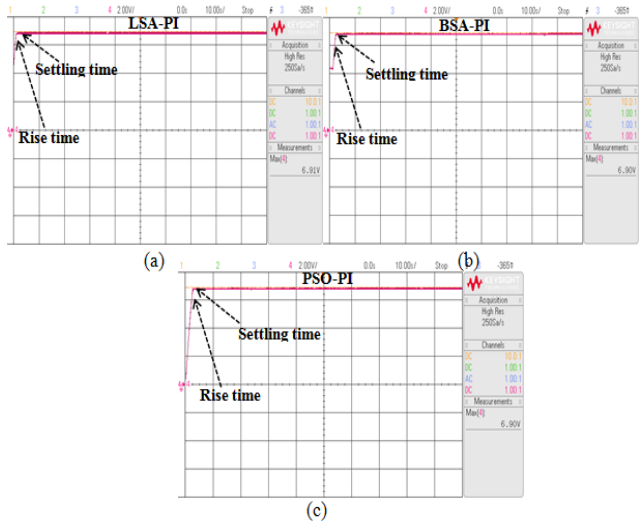

FIGURE 24. Experimental results of the LSA-PI (a), BSA-PI (b) and PSO-PI (c) controllers based on the rise and settling times with an input of 150 mV.

3) SIMULATION AND EXPERIMENTAL RESULTS BASED ON THE SETTLING TIME AND RISE TIME WITH AN INPUT OF 250 MV

The controller is again tested by changing the input to 250 mV. The difficult part of the vibration-based PEHSC is the energy extracted from the PBG due to the unsudden behavior of a vibration that is not stable and fixed. Again, the LSA-PI, BSA-PI, and PSO-PI controllers are tested by changing the input to 250 mV for multiple loads.

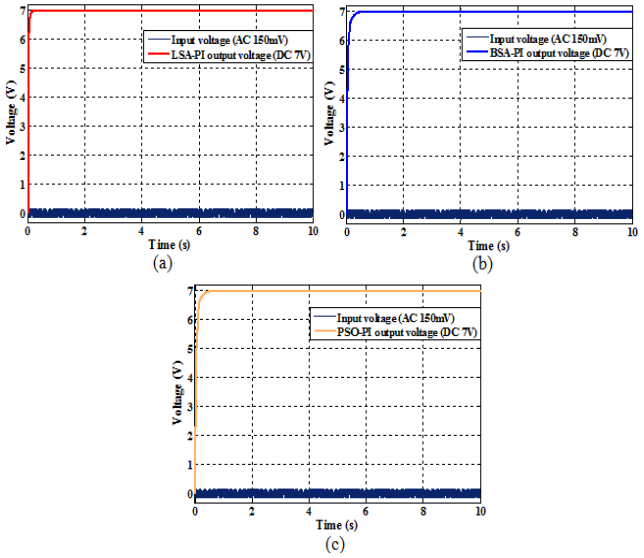

FIGURE 25. Simulation outcomes of PEHSC using the LSA-PI (a) BSA-PI (b) and PSO-PI (c) controllers.

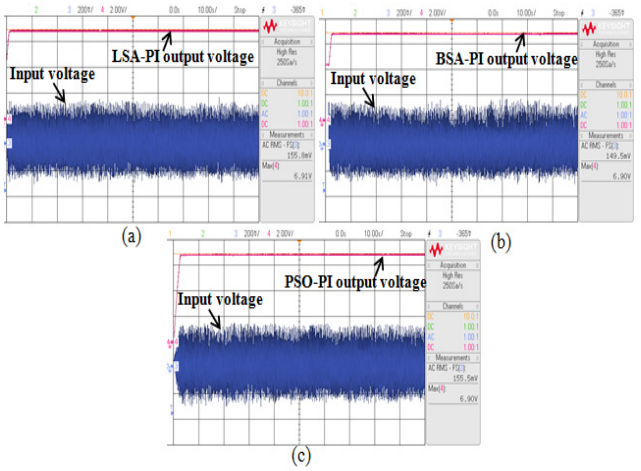

FIGURE 26. Hardware outcomes of an integrated PEHS converter using the LSA-PI (a) BSA-PI (b) and PSO-PI (c) controllers with an input of 150 mV.

TABLE 5. Comparison between simulation and hardware implementation results for 150 mV.

Frequency	Vrms (Input)	Simulation Result	Output in Hardware implementation Results	Optimization techniques
30 Hz	150 mV	7 V	6.91 V 6.90 V 6.90 V	LSA-PI BSA-PI PSO-PI

For validation, the performance of the LSA-PI controller is compared with that of BSA-PI and PSO-PI based on the rising and settling times to confirm the stability of the proposed controller. The feedback of the PEHSC simulation results using the LSA-PI, BSA-PI, and PSO-PI controllers is presented in Fig. 27. From Fig. 27, it is observed that the LSA-PI voltage controller for PEHSC gains the best optimal result during

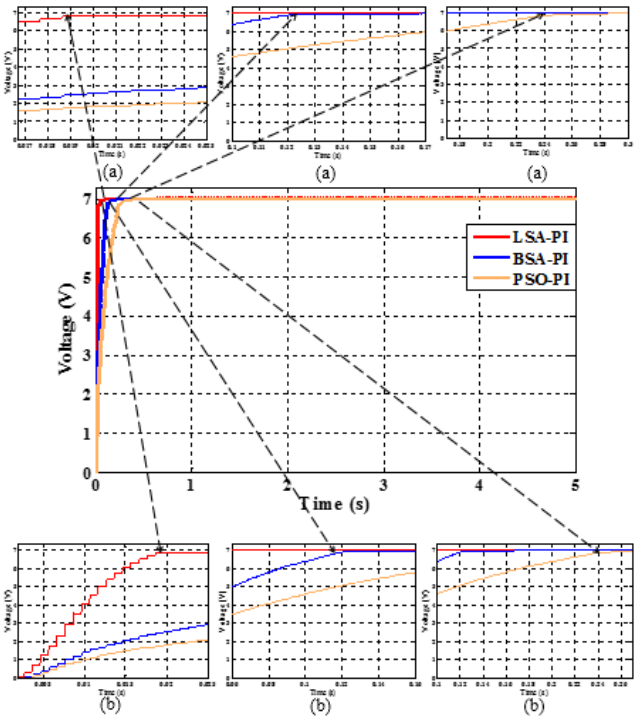

FIGURE 27. Simulation results of the LSA-PI, BSA-PI and PSO-PI controller with settling time (a) and rise for an input of 250 mV.

the input change based on the rising and setting times. The hardware implementation measured output results agree with the simulated outcomes as presented in Fig. 28. Table 6 shows the verification of the optimized outcomes for each algorithm.

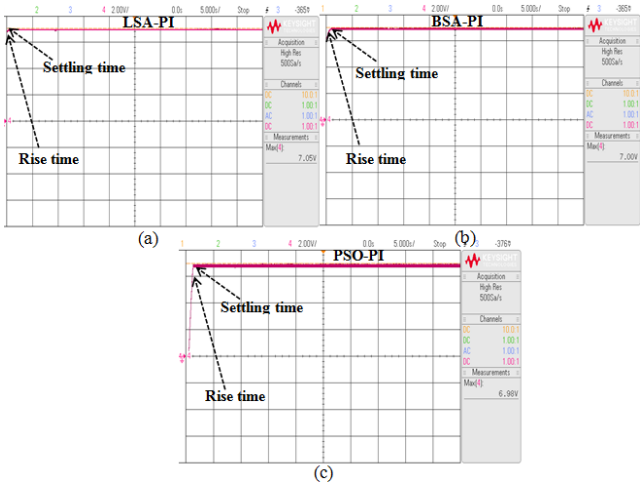

FIGURE 28. Experimental results of the LSA-PI (a), BSA-PI (b) and PSO-PI (c) controllers based on the rise and settling time for an input of 250 mV.

4) SIMULATION AND HARDWARE RESULTS OF A PEHSC FOR AN INPUT OF 250 MV

This work further evaluates the simulation and hardware results of a PEHSC by changing the input voltage to test the outcomes of the proposed PEHSC using optimization techniques. The simulation outcomes of the LSA-PI, BSA-PI and PSO-PI methods are presented in Fig. 29 (a), (b) and (c), respectively. In all the figures, the voltage output characteristics of each method are almost comparable without a major difference. Fig. 29 (a), (b) and (c) shows the input AC sinusoidal Vrms 250 mV produced from the PBG and the step-up to the optimal output voltage of 7 V DC. However, Fig. 29 (a) shows that the curve initially bends, but after 0.0187 s, it becomes stable. Fig. 29 (b) and (c) show that the curve is becoming bent; initially, some time is required to reach the optimal voltage, but in BSA-PI and PSO-PI after 0.124 s and 0.259 s, respectively, the curve becomes stable. The peak overshoot value is comparable for the three methods. The experimentally measured outcomes agree with the simulated results presented in Fig. 30 (a), (b) and (c). The comparison between the simulation and hardware implementation results of PEHSC are provided in Table 7. Therefore,

TABLE 6. Verification of the outcomes obtained for the LSA-PI, BSA-PI and PSO-PI controllers for an input of 250 mV.

Algorithms	Rise Time	Settling Time	Peak over shoot	Steady state Error
LSA-PI	0.0159 s	0.0187 s	0%	0.1
BSA-PI	0.199 s	0.124 s	0%	0.1
PSO-PI	0.244 s	0.259 s	0%	0.1

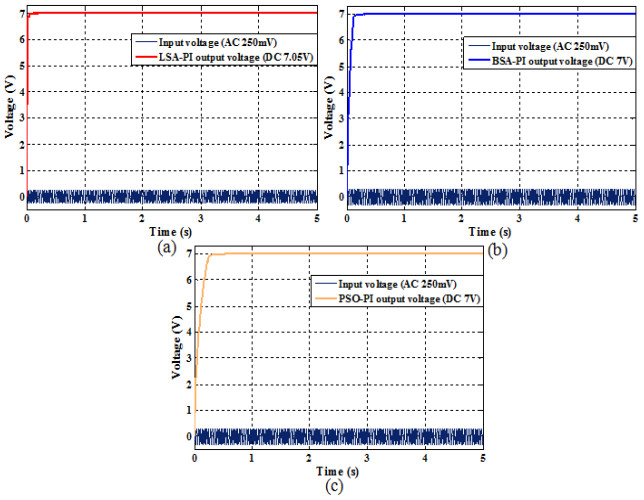

FIGURE 29. Simulation results of an integrated PEHSC using the LSA-PI (a) BSA-PI (b) and PSO-PI (c) controllers for an input of 250 mV.

TABLE 7. Comparison between simulation and hardware implementation results.

Frequency	Vrms (Input)	Simulation Result	Output in Hardware implementation Results	Optimization techniques
30 Hz	250 mV	7.05 V	7.05 V 7 V 6.98 V	LSA-PI BSA-PI PSO-PI

TABLE 8. Comparison of the results with the current and conventional work.

Component	[23] [10]	[15]	[23]	[25]	[26]	[31]	This Work
Algorithm	-	-	BSA	LSA	-	-	LSA-PIVC
Vin (Input voltage)	2.5 V	40 mV	0.3 V	0.3 V	0.54 V	0.7 V	150-250 mV
Vo (Output voltage)	5 V	4.1 V ~ 5 V	6.06 V	7 V	3.3 V	5 V	7.05 V
Switching Frequency	50.39 kHz	100 kHz	10 kHz	10 kHz	-	229.6 Hz	10 kHz
Load	-	-	Resistive load	Resistive load	60 Ω	61 kΩ	1.5 MΩ, 1 MΩ, 1000 kΩ, 500 kΩ, 300 kΩ
Duty	-	-	-	-	50%	-	95%
Application	EH	EH	Micro devices	EH	EH	EH	Low power

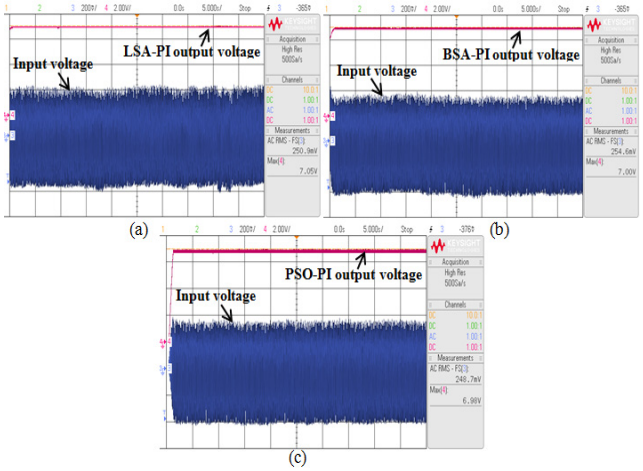

FIGURE 30. Experimental results of an integrated PEHSC using an LSA-PI (a), BSA-PI (b) and PSO-PI (c) controller with an input of 250 mV.

from these results, it is observed that the outcomes of the LSA-PI voltage controller are much better than those of the other methods for each feature.

VII. COMPARISON WITH EXISTING METHOD

Table 8 shows the results of the PEHSC are verified between the proposed and conventional work using LSA-PI controllers based on the voltage, switching frequency, converter efficiency, and controller techniques. The comparison also covers the efficiency, the number of components needed and the power loss. Moreover, the comparison focuses on the advantages and disadvantages of the PEHSC controller.

Some researchers have designed a step-up converter for PEHS, but no one has used optimization techniques. In [26], [31], and [32], the work is presented with a step-up converter to raise the performance of the output voltage for PEHSC using a PI controller, avoiding an optimization technique. The study in [31] designed a parallel-SSHI rectifier for piezoelectric energy harvesting applications. The model boosts 5 V DC with an input of 0.7 V AC. The drawback of this model is that it is not suitable for various loads or for a long life without a converter. However, the compensation circuit is too complicated without an added converter. The work in [26] is presented with a step-up and flyback converter to raise the outcomes of PEHSC without using an optimization algorithm. The developed model boosts 3.3 V DC with an input of 0.54 V AC. The drawback of this work is that it is not implemented at the hardware level. In [10], the study is presented in a flyback converter to raise the outcomes of PEHSC. The model increases 5 V DC with an input of 2.5 V AC. The drawback of this work is that it did not report the duty cycle of the converter and it did not validate the hardware level. The study in [15] designed a DC-DC boost converter to increase the output voltage for the EH system, and the model boosts 4.1 V ~ 5 V DC with an input of 40 mV AC and 2.7 V AC. However, this work did not report the duty and the voltage level was not very high according to input. The study in [23] proposed a BSA-PI controller to increase the output voltage of the PEHSC. The developed model boosts 6.06 V DC with an input of 0.3 V AC. However, the limitation of this work is that the output voltage efficiency is low. The work in [25] presented an LSA method for improving the PIVC for PEHSC. However, this model did not report the duty and the work was not implemented in the hardware level.

VIII. CONCLUSION

This study proposed a new framework of the vibration-based PEHSC based on an optimization technique applied for developing an optimal PIVC. This study also presented a signal-phase closed loop boost converter control system development using a PIVC for enhancement of the PEHSC. A DSP-type of controller platform named the dSPACE DS1104 controller board was used, to which the developed converter control algorithm was linked and loaded. In the traditional PIVC, a trial and error method is generally used to achieve optimal values for the K_p and K_i. This technique is time consuming and does not lead to satisfactory solutions. Therefore, to avoid the conventional trial-and-error process, a new method for a PEHSC using a meta-heuristic optimization method known as the LSA is proposed in this study to obtain the optimal parameter values of K_p and K_i for designing a PIVC. The proposed LSA also used MAE as an

objective function to reduce the optimization error. A wide comparative study with the LSA, BSA, and PSO algorithms was performed to validate and compare the performance of the LSA in finding the global minimum value of the objective function for the MAE. The proposed LSA exhibits suitable investigation, utilization and convergence characteristics.

The LSA-based PIVC of the PEHSC generates a great enhancement in reducing the output error of the converter, and a controlled PWM signal is used to alter MOSFET switching via the suitable feedback-based rise time and settling time under numerous loads. Finally, the experimental results conducted in the laboratory are shown to verify and justify the proposed optimum PI voltage controller using the LSA for the PEHSC controller. The experimental results are obtained to assess the efficiency and robustness of the proposed PEHSC controller. The simulation and hardware outcomes of this method are verified via the outcomes of the BSA-PI and PSO-PI to confirm the results. The results clearly show that the LSA-PI controller outperforms the BSA-PI and PSO-PI controllers in terms of rising time, settling time, stability, boost maximum voltage, converter efficiency, and response time. Finally, this hardware effectively increases the voltage 150 mV $\sim$ 250 mV, with 30 Hz AC to 7.05 V DC. The output voltage is strongly controlled at 7.05 V by a closed-loop using an LSA-PIVC, which is appropriate for low voltage applications.

REFERENCES

[1] T. Ruan, Z. J. Chew, and M. Zhu, "Energy-aware approaches for energy harvesting powered wireless sensor nodes," *IEEE Sensors J.*, vol. 17, no. 7, pp. 2165–2173, Apr. 2017.

[2] S. Kosunalp, "A New energy prediction algorithm for energy-harvesting wireless sensor networks with Q-learning," *IEEE Access*, vol. 4, pp. 5755–5763, 2016.

[3] M. Dini, A. Romani, M. Filippi, and M. Tartagni, "A nanopower synchronous charge extractor IC for low-voltage piezoelectric energy harvesting with residual charge inversion," *IEEE Trans. Power Electron.*, vol. 31, no. 2, pp. 1263–1274, Feb. 2016.

[4] A. M. Khalatkar and V. K. Gupta, "Piezoelectric energy harvester for low engine vibrations," *J. Renew. Sustain. Energy*, vol. 9, no. 2, p. 024701, Mar. 2017.

[5] G. Ali, J. Wagner, D. Moline, and T. Schweisinger, "Energy harvesting from atmospheric variations—Theory and test," *Renew. Energy*, vol. 74, pp. 528–535, Feb. 2015.

[6] M. Hassanalieragh, T. Soyata, A. Nadeau, and G. Sharma, "UR-SolarCap: An open source intelligent auto-wakeup solar energy harvesting system for supercapacitor-based energy buffering," *IEEE Access*, vol. 4, pp. 542–557, 2016.

[7] L. W. Liu, Q. Zhang, Y. Chen, M. A. Teeti, and R. Das, "Wireless energy harvesting by direct voltage multiplication on lateral waves from a suspended dielectric layer," *IEEE Access*, vol. 5, pp. 21873–21884, 2017.

[8] R. Mohamed, M. R. Sarker, and A. Mohamed, "An optimization of rectangular shape piezoelectric energy harvesting cantilever beam for micro devices," *Int. J. Appl. Electromagn. Mech.*, vol. 50, no. 4, pp. 537–548, Mar. 2016.

[9] Y. Zhao, K. Wang, and M. Guan, "An adaptive boost converter for low voltage piezoelectric energy harvesting," *Ferroelectrics*, vol. 502, no. 1, pp. 107–118, Nov. 2016.

[10] B. Khemmanee and D. Isarakorn, "Low-cost energy management circuit base on primary feedback self-oscillating flyback converter for piezoelectric energy harvesting," in *Proc. 18th Int. Conf. Elect. Mach. Syst. (ICEMS)*, Oct. 2015, pp. 1035–1038.

[11] Z. J. Chew and M. Zhu, "Adaptive maximum power point finding using direct $V_{oc}/2$ tracking method with microwatt power consumption for energy harvesting," *IEEE Trans. Power Electron.*, vol. 33, no. 9, pp. 8164–8173, Sep. 2018.

[12] J. Kang, Y. Kim, J. Yoo, and L. Hwang, "Piezoelectric energy harvesting using PMW-PNN-PZT ceramics for DC-DC converter application," *Ferroelectr. Lett. Sect.*, vol. 42, nos. 4–6, pp. 87–96, Dec. 2015.

[13] A. H. Alameh and F. Nabki, "A 0.13 μm CMOS power conditioning circuit for piezoelectric vibration energy harvesters," in *Proc. IEEE 60th Int. Midwest Symp. Circuits Syst. (MWSCAS)*, Aug. 2017, pp. 839–842.

[14] T. Oh, S. K. Islam, G. To, and M. Mahfouz, "Powering wearable sensors with a low-power CMOS piezoelectric energy harvesting circuit," in *Proc. IEEE Int. Symp. Med. Meas. Appl. (MeMeA)*, May 2017, pp. 308–313.

[15] H. Yu, J. Zhou, L. Deng, and Z. Wen, "A vibration-based MEMS piezoelectric energy harvester and power conditioning circuit," *Sensors*, vol. 14, no. 2, pp. 3323–3341, Feb. 2014.

[16] N. ur Rahman and M. N. Alam, "Active vibration control of a piezoelectric beam using PID controller: Experimental study," *Latin Amer. J. Solids Struct.*, vol. 9, no. 6, pp. 657–673, Dec. 2012.

[17] P. D. Ngo and Y. C. Shin, "Gain estimation of nonlinear dynamic systems modeled by an FBFN and the maximum output scaling factor of a self-tuning PI fuzzy controller," *Eng. Appl. Artif. Intell.*, vol. 42, pp. 1–15, Jun. 2015.

[18] A. Harrag and S. Messalti, "Variable step size modified P&O MPPT algorithm using GA-based hybrid offline/online PID controller," *Renew. Sustain. Energy Rev.*, vol. 49, pp. 1247–1260, Sep. 2015.

[19] R. S. Rajesh Babu, M. E. S. Deepa, and M. E. S. Jothivel, "A closed loop control of quadratic boost converter using PID controller," *IJE Trans. B, Appl.*, vol. 27, no. 11, pp. 1653–1662, Jan-2014.

[20] J. C. Basilio and S. R. Matos, "Design of PI and PID controllers with transient performance specification," *IEEE Trans. Educ.*, vol. 45, no. 4, pp. 364–370, Nov. 2002.

[21] C. Elmas and T. Yigit, "Genetic algorithm based on-line tuning of a PI controller for a switched reluctance motor drive," *Electr. Power Compon. Syst.*, vol. 35, no. 6, pp. 675–691, Mar. 2007.

[22] P. Farhang, A. M. Drimus, and S. Mátéfi-Tempfli, "New technique for voltage tracking control of a boost converter based on the PSO algorithm and LTspice," in *Proc. 56th Int. Sci. Conf. Power Elect. Eng. Riga Tech. Univ. (RTUCON)*, Oct. 2015, pp. 1–6.

[23] M. R. Sarker, A. Mohamed, and R. Mohamed, "A new method for a piezoelectric energy harvesting system using a backtracking search algorithm-based PI voltage controller," *Micromachines*, vol. 7, no. 10, p. 171, Sep. 2016.

[24] H. Shareef, A. A. Ibrahim, and A. H. Mutlag, "Lightning search algorithm," *Appl. Soft Comput.*, vol. 36, pp. 315–333, Nov. 2015.

[25] M. R. Sarker, A. Mohamed, and R. Mohamed, "Improved proportional-integral voltage controller for a piezoelectric energy harvesting system converter utilizing lightning search algorithm," *Ferroelectrics*, vol. 514, no. 1, pp. 123–145, Jul. 2017.

[26] M. G. Mostafa, S. M. A. Motakabber, and M. I. Ibrahimy, "Design and analysis of a buck-boost converter circuit for piezoelectric energy harvesting system," in *Proc. Int. Conf. Comput. Commun. Eng. (ICCCE)*, Jul. 2016, pp. 204–207.

[27] J. A. N. D. Ang *et al.*, "Development of a DC-DC converter with Current Mode Control for multi-source renewable energy harvesting system," in *Proc. IEEE Region 10 Conf. (TENCON)*, Nov. 2016, pp. 556–559.

[28] Y. Nishikawa, N. Sannomiya, T. Ohta, and H. Tanaka, "A method for auto-tuning of PID control parameters," *Automatica*, vol. 20, no. 3, pp. 321–332, May 1984.

[29] C. Yanbo and K. W. E. Cheng, "Real-time simulation and experiment platform for switched reluctance motor," in *Proc. 2nd Int. Conf. Power Electron. Syst. Appl.*, Nov. 2006, pp. 244–249.

[30] T. Chai and R. R. Draxler, "Root mean square error (RMSE) or mean absolute error (MAE)—Arguments against avoiding RMSE in the literature," *Geosci. Model Dev.*, vol. 7, no. 3, pp. 1247–1250, Jun. 2014.

[31] D. A. Sanchez, J. Leicht, F. Hagedorn, E. Jodka, E. Fazel, and Y. Manoli, "A parallel-SSHI rectifier for piezoelectric energy harvesting of periodic and shock excitations," *IEEE J. Solid-State Circuits*, vol. 51, no. 12, pp. 2867–2879, Dec. 2016.

[32] H. Wang, Y. Tang, and A. Khaligh, "A bridgeless boost rectifier for low-voltage energy harvesting applications," *IEEE Trans. Power Electron.*, vol. 28, no. 11, pp. 5206–5214, Nov. 2013.

MAHIDUR R. SARKER received the B.Sc. degree in computer science and engineering from Southeast University, Dhaka, Bangladesh, and the M.Sc. degree in microengineering and nanoelectronics and the Ph.D. degree in electrical, electronic, and systems engineering from the Universiti Kebangsaan Malaysia (UKM), Bangi, Malaysia, in 2013 and 2017, respectively. He is currently a Post-Doctoral Research Fellow with the Center for Integrated Systems Engineering and Advanced Technologies, UKM. His research interests include piezoelectric energy harvesting, power electronics, artificial intelligence, and model optimization.

RAMIZI MOHAMED received the B.Eng. degree (Hons.) from the University of Salford, U.K., the M.Sc. degree from Universiti Kebangsaan Malaysia (UKM), and the Ph.D. degree from Southampton University, U.K. He is currently a Senior Lecturer with the Center for Integrated Systems Engineering and Advanced Technologies, UKM. His research interests are in transformer condition monitoring, solar hybrid energy harvesting, and piezoelectric energy harvesting.

MOHAMAD HANIF MD. SAAD received the B.Eng. (Hons.) and Ph.D. degrees from Universiti Kebangsaan Malaysia (UKM) and the M.Sc. degree in mechatronics from the National University of Singapore. He is currently a Senior Lecturer with the Center for Integrated Systems Engineering and Advanced Technologies, UKM. His research interests include artificial intelligence, intelligent systems, and complex event processing.

AZAH MOHAMED (M'88–SM'05) received the B.Sc. degree from the University of London, in 1978 and the M.Sc. and Ph.D. degrees from the University of Malaya, in 1988 and 1995, respectively. She is currently a Senior Professor with the Center for Integrated Systems Engineering and Advanced Technologies, Universiti Kebangsaan Malaysia. Her main research interests are in power system security, power quality, and artificial intelligence.